Decoupled Modulation Concept for Three-to-Single-Phase Direct AC/AC Modular Multilevel Converters for Railway Interties

Michail Vasiladiotis[1], Alexandre Christe[2], Tobias Geyer[3], Alexander Faulstich[1]
[1]ABB Switzerland Ltd., Austrasse, 5300 Turgi, Switzerland
[2]École Polytechnique Fédérale de Lausanne (EPFL), 1015 Lausanne, Switzerland
[3]ABB Corporate Research, Segelhofstrasse 1K, 5405 Baden-Dättwil, Switzerland
Emails: michail.vasiladiotis@ch.abb.com, alexandre.christe@epfl.ch,
tobias.geyer@ch.abb.com, alexander.faulstich@ch.abb.com

Keywords

≪Multilevel converters≫, ≪AC/AC converter≫, ≪Modulation strategy≫, ≪Converter control≫, ≪Harmonics≫.

Abstract

This paper presents a new modulation concept for three-to-single-phase direct AC/AC modular multilevel converter-based railway interties. The concept minimizes the inherent harmonic coupling between the two grid sides and is therefore particularly suited to operation at very low cell numbers and switching frequencies. Moreover, it facilitates the use of specific modulation methods, such as optimized pulse patterns. Additional aspects, such as the influence of cell capacitor voltage ripple as well as circulating current control, are also considered. The latter can be integrated into the control concept in a straightforward manner.

Introduction

The three-to-single-phase direct AC/AC modular multilevel converter (MMC), which is illustrated in Fig. 1, can be used for the interconnection of a three-phase utility grid, e.g., 50 Hz, with a single-phase railway supply, e.g., $16\,^{2}/_{3}$ Hz (synchronous) or 16.7 Hz (asynchronous) [1-3]. The latter is commonly used in several European countries. The converter features six branches, which consist of identical series-connected cells. The cells need to be bipolar–providing positive and negative voltages–and can be implemented in the simplest case as full-bridges.

The authors of [4,5] have proposed control approaches for the inner dynamics of such a direct MMC, which are based on capacitor voltage ripple estimation. The operation and converter control under grid unbalances, as well as their impact on cell capacitor sizing, is the focus of [6]. Integration of energy storage elements on a cell level for providing additional services, such as load-leveling, is presented in [7]. Publications [8,9] discuss converter design and semiconductor-related topics. Finally, the use of such a converter in the frame of wind turbine generation systems is introduced by [10].

In general, the advantages of an MMC over conventional converter topologies are widely documented, especially in the field of high-voltage direct current (HVDC) systems. Compared to these applications, however, such medium voltage railway intertie converters require a much lower number of cells. Moreover, system efficiency is of great significance, implying that it is preferable to minimize the converter losses by reducing the switching frequency. In such conditions, maintaining the converter's harmonic performance becomes a challenging task. Therefore, the chosen modulation method has a considerable effect on the global system performance.

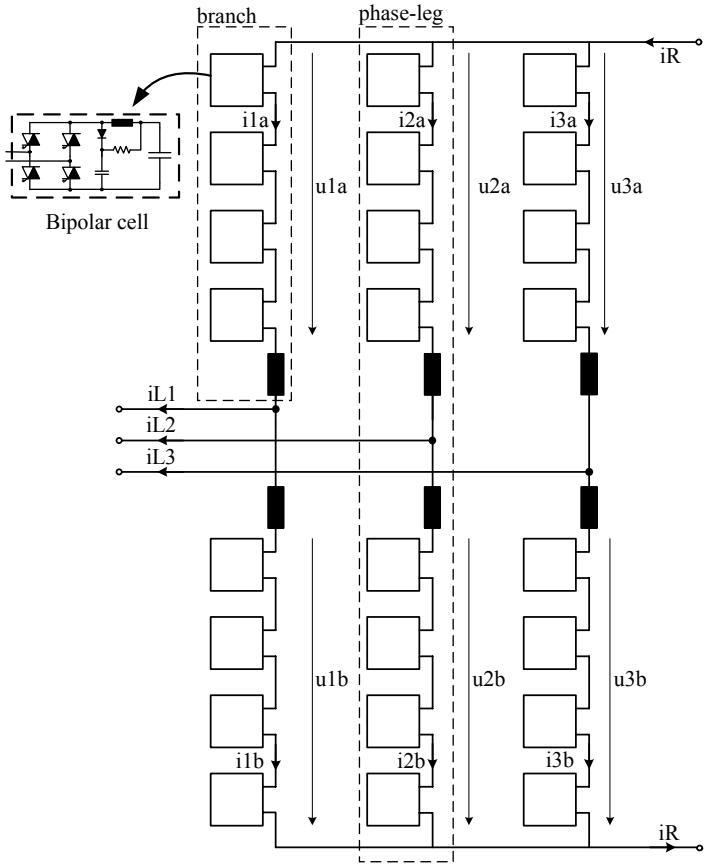

Fig. 1: The three-to-single-phase direct AC/AC modular multilevel converter.

This paper proposes a new approach to the modulation of such direct MMCs. Instead of a 'per branch' modulation (further referred to as coupled modulation concept), it is suggested to use a 'per side' modulation (further referred to as decoupled modulation concept). This means that the single- and three-phase sides are modulated independently from one another. The modulator outputs from both sides are then mapped to switching positions of each branch that are then fed to the well-known sorting and selection algorithm, as described in the following sections.

The decoupled modulation concept

The direct AC/AC MMC can be modulated by combining the different time-varying quantities resulting from the different control layer structures, and feeding them into the same modulator. The voltage references for the upper and lower branches of the k-th phase-leg can be calculated as

$$u^*_{ka}(t) = \frac{u^*_R(t)}{2} - u^*_{Lk}(t) - u^*_{cm}(t) - u^*_{circk}(t) \tag{1}$$

$$u^*_{kb}(t) = \frac{u^*_R(t)}{2} + u^*_{Lk}(t) + u^*_{cm}(t) - u^*_{circk}(t) \tag{2}$$

where k = 1,2,3 corresponds to the different phases, $u^*_R(t)$, $u^*_{Lk}(t)$ denote the references for the railway and utility grid side voltages, respectively, $u^*_{cm}(t)$ is a freely chosen common-mode voltage component and $u^*_{circk}(t)$ is the reference from the MMC inner control/balancing actions.

This implementation results in a harmonic interaction between the two networks, especially at low cell numbers and switching frequencies. Figure 2 demonstrates this effect for the case of 8 cells per branch using the simplest case of nearest level modulation (NLM) and assuming ideal conditions, i.e., without considering any cell capacitor voltage ripple.

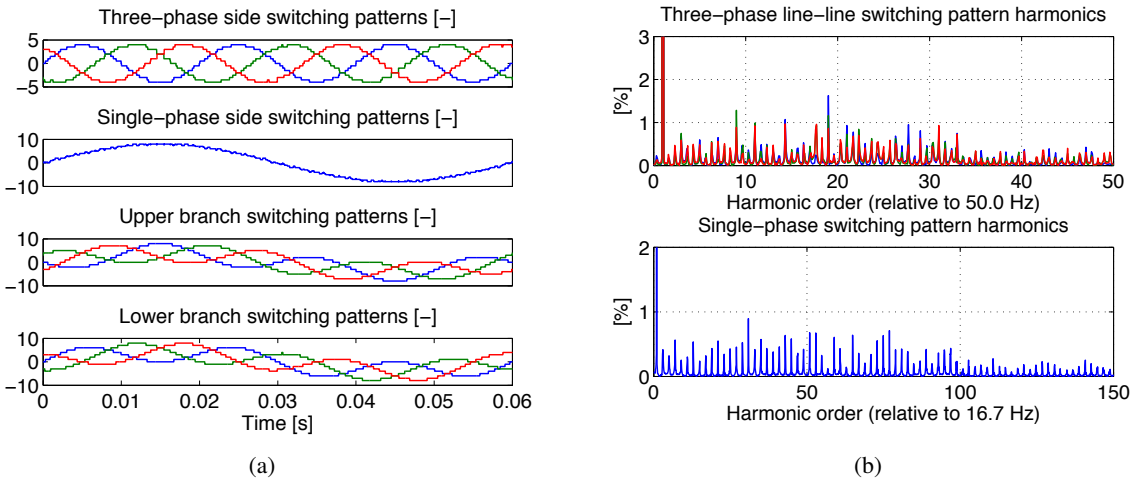

(a) (b)

Fig. 2: 'Per branch' (coupled) modulation under ideal conditions with $N = 8$ cells per branch, NLM and single-phase frequency of $f_{1\phi} = 16.7$ Hz. (a) Switching patterns: the modulator produces the branch signals of the two lower graphs, which result in the equivalent patterns on each side as shown in the two upper graphs. (b) Harmonic spectrum on both converter sides. Resulting average switching frequency is $\overline{f_{sw}} \approx 50$ Hz.

It is clear that such a 'per branch' modulation does not guarantee quarter-wave symmetry in the switching patterns on the three- and single-phase sides, which has a considerable impact on the harmonic spectrum. In general, when the ratio between the two grid frequencies (denoted further on as $f_{3\phi}$ and $f_{1\phi}$) is described by the following relation

$$x \cdot f_{1\phi} = f_{3\phi}, \quad x \in \mathbb{Q}, \quad x > 0 \tag{3}$$

interharmonics will appear on both sides. In addition, and as shown in Fig. 2(b), the harmonic magnitude between the three phases varies significantly. The latter poses significant challenges in fulfilling the harmonic requirements when the cell number and switching frequency are low.

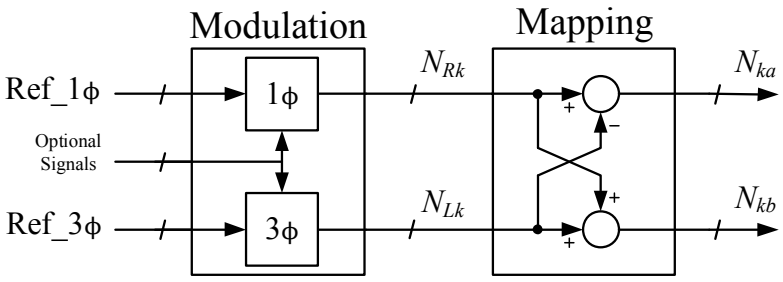

Fig. 3: The general case of the proposed 'per side' decoupled modulation concept.

To overcome this problem, a new modulation approach is proposed, whose simplified block diagram is shown in Fig. 3. Each side is modulated independently, having received an appropriate reference signal from the upper layer application controllers, here denoted as Ref_1ϕ and Ref_3ϕ, respectively. In the general case, these could be scalar or vector signals such as time-varying voltage or virtual flux quantities, modulation indices with angular references, etc. Optional signals, such as measurements or system parameters, might be needed for additional compensating actions on a modulation level. The modulation produces the integer command signals N_{Rk} and N_{Lk} for each side. It is noted that in order to achieve single-phase side interleaving and/or circulating current control, N_{Rk} needs to be calculated per k-th phase-leg and is therefore depicted here as a vector. As a next step, the signals N_{Rk} and N_{Lk} have to

be mapped to branch-level integer command signals N_{ka} and N_{kb}, where 'a' refers to the upper and 'b' to the lower branches of the k-th phase-leg. The latter will eventually be fed to a conventional sorting and selection algorithm ensuring balancing between the individual cell voltages within the same branch.

Similarly to Fig. 2, the results of such a 'per side' modulation for ideal conditions, i.e., without considering the cell capacitor voltage ripples, are illustrated in Fig. 4. It is shown that the decoupled modulation concept using NLM leads to quarter-wave symmetry on both sides. As a result, the respective harmonic spectra are free of any interharmonics. Furthermore, the decoupled modulation is insensitive to factors such as asynchronous operation, different possible phase-shifts between the three- and single-phase grid voltages, etc. It is noted that the 'fundamental' switching frequency is now defined as $f_{3\phi} + f_{1\phi}$. Lower switching frequencies can be achieved according to the chosen modulation methods for each converter side.

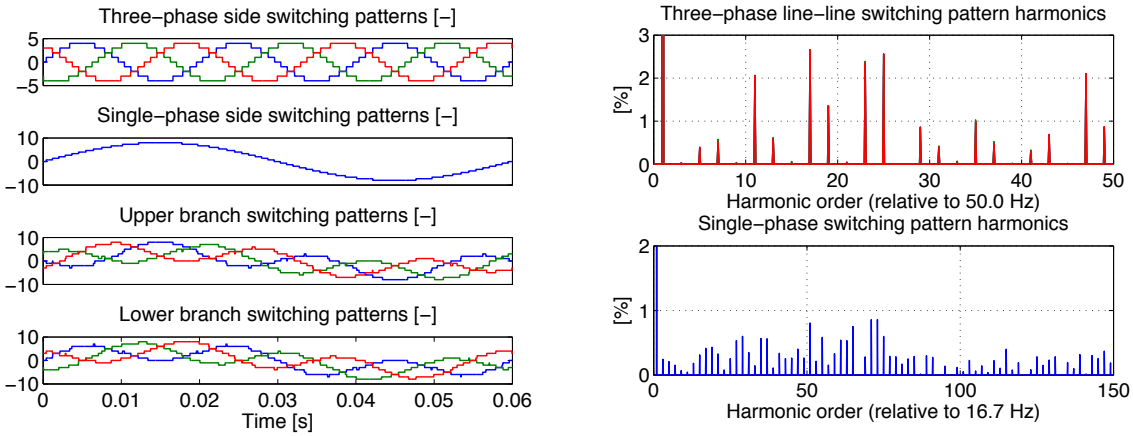

(a) (b)

Fig. 4: 'Per side' (decoupled) modulation under ideal conditions with $N = 8$ cells per branch, NLM and single-phase frequency of $f_{1\phi} = 16.7$ Hz. Interleaving towards the single-phase side is also used. (a) Switching patterns: the modulator now produces the signals of the two upper graphs, which are mapped to their equivalent patterns of the six converters branches as shown in the two lower graphs. (b) Harmonic spectrum on both converter sides. Resulting average switching frequency is now $\overline{f_{sw}} \approx 66.7$ Hz.

As already mentioned, the modulation on the single-phase converter side can be enhanced by interleaving between the three individual converter phase-legs, which is also considered in Fig. 4. Such an increased voltage resolution leads to a significantly improved single-phase harmonic spectrum. However, the interleaving method needs to be defined appropriately, so as not to lead to large circulating currents between the converter phase-legs. In any case it is noted that the decoupled modulation concept will have an impact on the branch reactor sizing.

Modulation and control

Capacitor voltage ripple influence

It has been shown that the decoupled modulation concept leads to the elimination of the inherent grid harmonic coupling due to the 'per branch' modulation. However, this holds only for ideal conditions. In reality, the voltage spectra will still be affected by the cell capacitor voltage ripples resulting from the energy variations that need to be buffered within the converter branches. In this particular application, and as opposed to the more common double-star DC/AC MMC case, there is an additional second-order power pulsation originating from the single-phase side, i.e., $2f_{1\phi} = 33.4$ Hz. The latter is expected to have an effect on the three-phase side spectrum as well. In fact, for every modulation-injected converter harmonic component of n-th order $f_{h,n}$, two sidebands are expected to appear at $f_{h,n} \pm 2f_{1\phi}$ as a result of convolution in the frequency domain [11]. The whole modulation process is further complicated by

the additional ripple frequencies reflected on the capacitor voltages, an analysis of which is presented in works such as [1,6]. An example of the capacitor voltage ripples in the converter is shown in Fig. 5(a). Therefore, the choice of the three-phase modulation scheme is especially very important.

Three-phase side modulation

At low switching frequencies, three-phase optimized pulse patterns (OPPs) constitute an attractive solution, since they facilitate the shaping of the harmonic spectrum. In this case, the concept of decoupled modulation is even a necessity, since it allows one to treat the two converter sides independently, which avoids the need to design and apply the OPP directly on a branch level. The latter would be nearly impossible to achieve, given the existence of two system frequencies but also an arbitrary phase-shift between the two networks in the case of asynchronous grid operation. Figure 5(b) shows an OPP calculated for 8 cells per branch and corresponding semiconductor modulating frequency of 56.25 Hz (number of switching transitions per quarter-wave $d = 9$), which is used in this work.

It is noted that OPPs targeting the minimization of the total harmonic distortion (THD) typically feature discontinuous switching angles, such as the one depicted in Fig. 5(b). The latter can be generally applied on a system in a closed-loop manner using advanced nonlinear control techniques, such as model predictive pulse pattern control (MP^{3}C). The main concept regards the real-time shifting of the offline pre-computed switching instants, in order to provide system disturbance rejection as well as fast instantaneous tracking of the virtual converter flux [12].

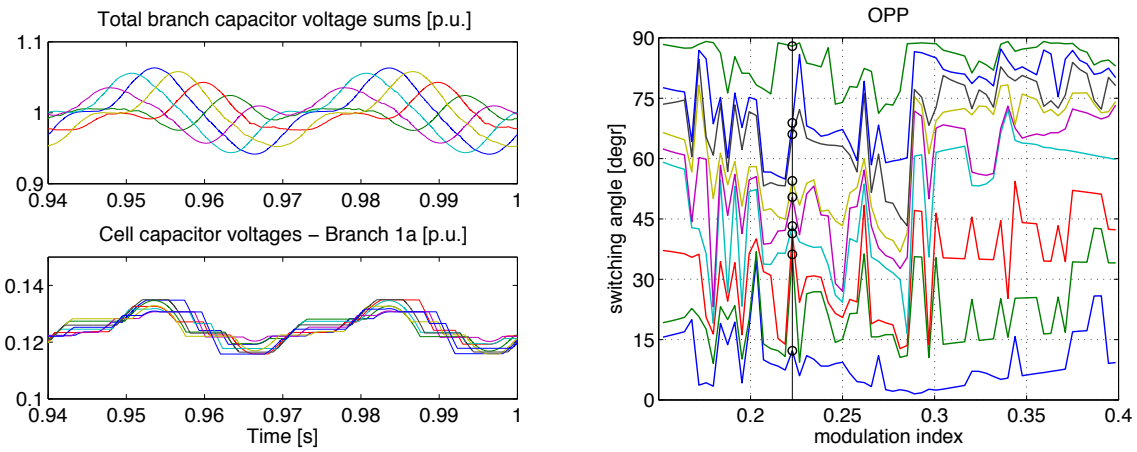

(a) (b)

Fig. 5: (a) Real-case capacitor voltage ripples (b) OPPs for $N = 8$ cells per branch and $d = 9$.

Single-phase side modulation and circulating current control

For the single-phase side, a discrete spectrum is preferable to facilitate fulfilling the individual frequency limits related to railway network interoperability. Therefore, the use of phase-shifted carrier PWM (PSC-PWM) is a solution. Interleaving between the three converter phase-legs is available, in order to increase the number of levels towards the single-phase side and therefore improve, even more, the harmonic performance. By choosing this modulation method, straightforward integration of the circulating current-driving voltages u^*_{circk} into the control and modulation scheme is offered. Circulating current control is therefore performed through three individual voltage references for the single-phase side, i.e., per converter phase-leg.

Figure 6 shows the modified block diagram for this specific example, which constitutes an implementation of the general concept illustrated in Fig. 3. The reference for the three-phase side comes in the form of a desired modulation index m^* and the angular reference θ^*. With this information, the OPP loader provides the corresponding switching sequence (pattern) along with the reference for the converter virtual flux in the stationary reference frame $\psi^*_{c,\alpha\beta}$, which is based on the ideal OPP's integration. The error of this reference value compared to the calculated converter virtual flux $\psi_{c,\alpha\beta}$ is fed to the MP^{3}C block

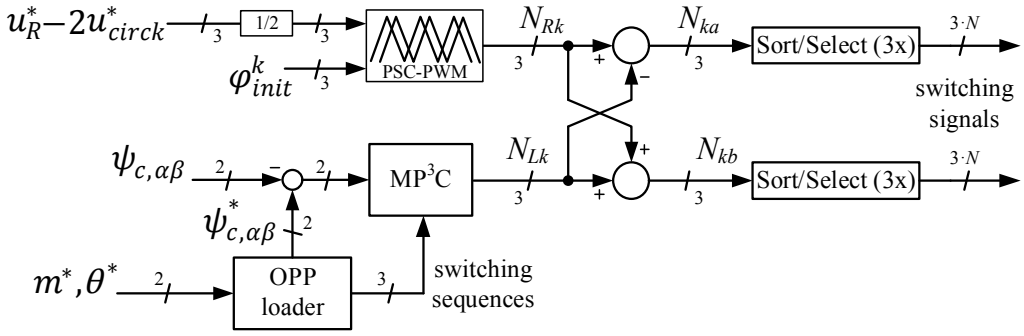

Fig. 6: Decoupled modulation using closed-loop controlled OPPs on the three-phase side and PSC-PWM on the single-phase side.

and shall be corrected by shifting the pulses of the ideal pattern accordingly. Finally, the output of the MP^{3}C block is the reference switching pattern towards the three-phase side.

The single-phase side modulator receives three voltage references. The latter is needed in order to contain the information for the circulating current-driving voltage u_{circk}^* as mentioned in previous paragraphs. Single-phase interleaving can be simply achieved by setting the initial carrier angles φ_{init}^k of the PSC-PWM block. The output of the latter is in the form of a vector containing the reference switching pattern of each phase-leg towards the single-phase side.

As a next step, the mapping function transforms the switching patterns of each side to respective ones for each of the six converter branches. In the final stage the branch switching patterns are fed to a typical sort and selection algorithm, which is responsible for producing the gate switching signals by assigning them to the cells in a way so as to maintain balanced voltages.

Results and comparative evaluation

The simulation results for the example shown in Fig. 6 are illustrated in Fig. 7. They refer to the nominal system active power with unity power factor on both converter sides and $N = 8$ cells per branch. The semiconductor modulating frequency towards the single-phase side has been chosen as 25 Hz, resulting in a total semiconductor switching frequency of 81.25 Hz. Fig. 7(a) shows the time-domain waveforms of the voltages towards the two grid sides. The three-phase line-line voltage exhibits quarter wave symmetry and the small asymmetries of the OPP are a result of the MP^{3}C algorithm trying to compensate for flux

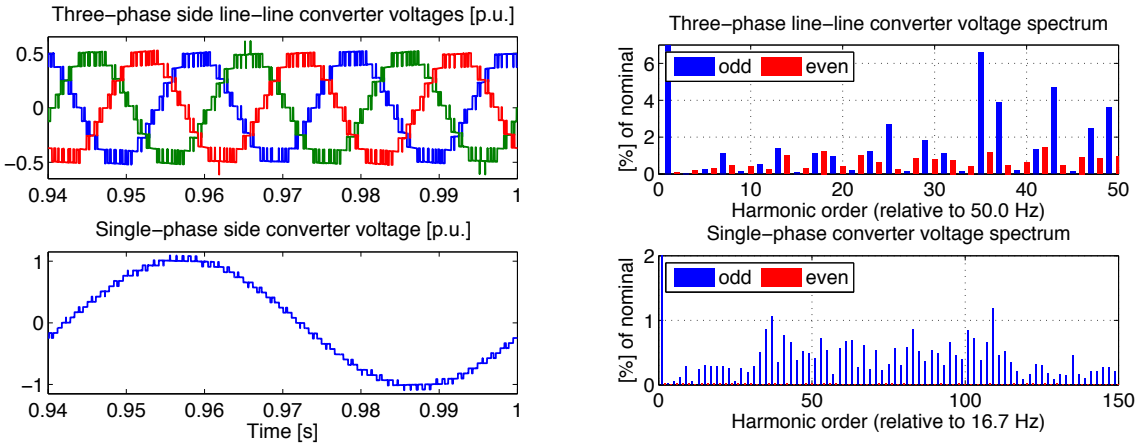

(a) (b)

Fig. 7: 'Per side' decoupled modulation using OPPs on the three-phase side and PSC-PWM on the single-phase side: (a) Time-domain voltage waveforms, (b) Converter voltage spectra.

ISBN: 9789075815276 et CFP17850-ART

errors and maintaining the ideal pattern.

The frequency-domain results of the converter voltages are illustrated in Fig. 7(b). It is noted that for all harmonic evaluations, the IEC 61000-4-7 standard is used for harmonic grouping. In addition, and for the three-phase side, the maximum harmonic amplitude between the three converter phases is illustrated. Finally, odd harmonics are depicted with blue and even harmonics with red.

The three-phase side OPPs are designed to minimize the voltage THD while keeping certain low-frequency harmonics below specified limits. The purpose for the latter is twofold. Initially, the first significant harmonic energy components are placed into a frequency range which reduces the size of a possible filter. Secondly, the additional interharmonics, originating from the capacitor voltage ripples (appearing here as even harmonics), can be kept under control. The single-phase side converter voltage features a discrete spectrum, which is in line with the PSC-PWM method used. The low-frequency harmonics originate from the second-order power pulsation in the cells. However, very low interharmonics/even harmonics exist.

The chosen 'per side' (decoupled) modulation example case is compared with two 'per branch' (coupled) modulation methods using the same semiconductor switching frequency and simulation operating point. Figure 8 presents the results for a PSC-PWM method with a carrier frequency of 81.25 Hz (equivalent branch PWM frequency of 1.3 kHz). It is clear that the lack of symmetry in the converter voltages as well as the capacitor voltage ripple influence, results in a lack of discrete PWM especially on the three-phase side. That leads to even harmonics that can be higher than their adjacent odd ones and are hard to limit from a modulation level. The single-phase suffers less from this due to the almost integer ratio between the two network frequencies in conjunction with the fact that a constant switching frequency modulator is used.

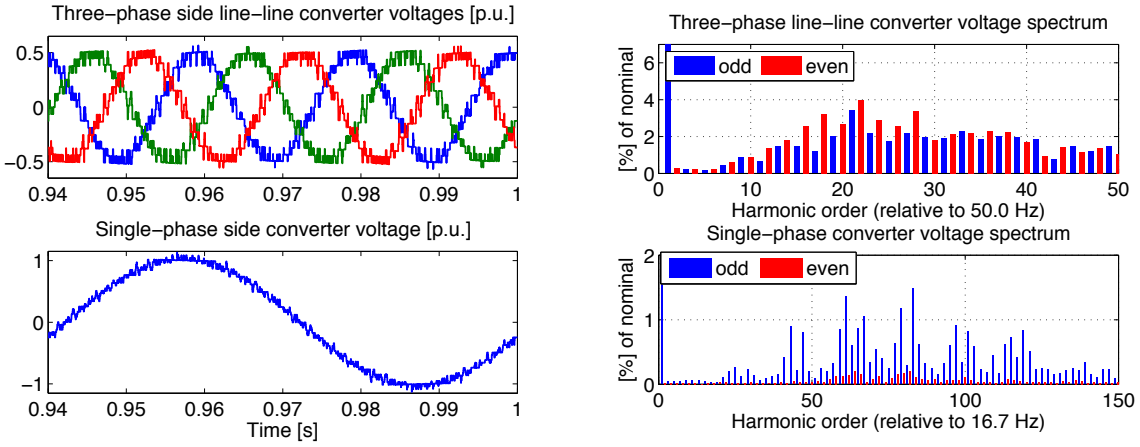

(a) (b)

Fig. 8: 'Per branch' coupled modulation using PSC-PWM: (a) Time-domain voltage waveforms, (b) Converter voltage spectra.

For low cell numbers and switching frequencies, carrier-based modulation methods do not achieve the desired performance. The proposed concept is also compared with a method based on setting hysteresis bands on the calculated converter branch virtual flux error [13]. Figure 9 shows the results for an average semiconductor switching frequency of 81.25 Hz tuned empirically by setting appropriately the hysteresis band. A stochastic nature of the voltage spectra is observed, similar to what would be expected in low switching frequency electric drive systems using hysteresis-based switching methods, such as direct torque control. In this case, also the single-phase side features even harmonics as a result of the non-repetitive switching pattern.

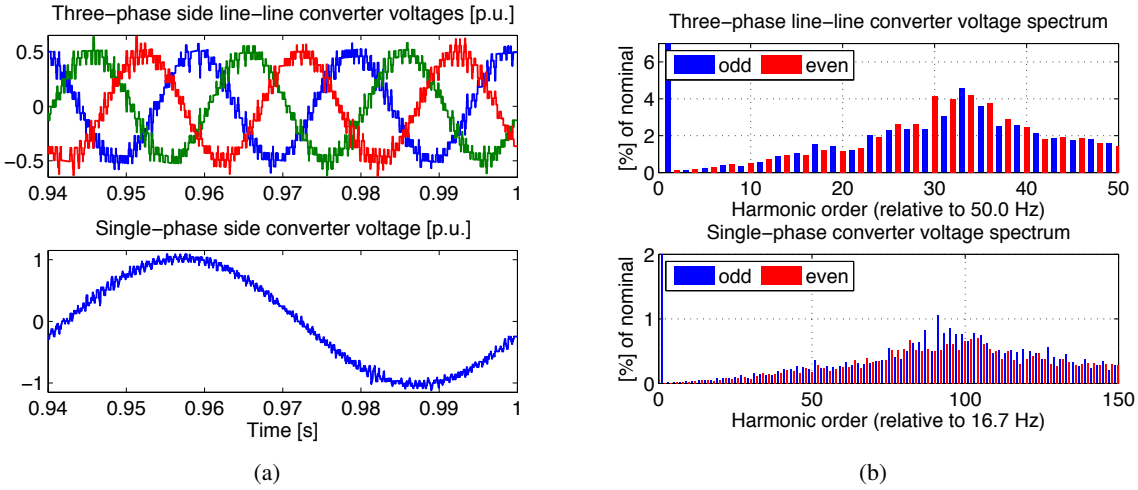

(a) (b)

Fig. 9: 'Per branch' coupled modulation using hysteresis bands for the converter virtual flux: (a) Time-domain voltage waveforms, (b) Converter voltage spectra.

Conclusion

It has been shown that it is difficult to achieve a good harmonic performance in a direct AC/AC MMC for railway interties under extreme conditions of low number of cells and switching frequencies using a 'per branch' coupled modulation concept and conventional methods. The proposed decoupled 'per side' modulation allows for a switching frequency reduction in such cases. Furthermore, this concept facilitates the use of modulation concepts, such as OPPs or space vector modulation (SVM), which are difficult to achieve with the coupled 'per branch' approach. The influence of the strong cell capacitor voltage ripple especially on the three-phase side can be further reduced by an active spectrum shaping with imposed harmonic limits, which is very important in such grid-connected applications. Finally, all the above implies an advantageous converter efficiency increase.

References

[1] M. Winkelnkemper, A. Korn, and P. Steimer, "A modular direct converter for transformerless rail interties," in *Proc. IEEE Int. Symp. Ind. Electron.*, pp. 562-567, July 4-7, 2010.

[2] R. Gruber, U. Halfmann, and M. Engel, "Statischer Bahnumrichter als selbstgeführter Direktumrichter in modularer Multilevel-Technik," in *VDE-Kongress*, Nov. 8-9, 2010.

[3] A. Steimel, "Power-electronic grid supply of AC railway systems," in *Proc. Int. Conf. Optim. Elect. Electron. Equip. (OPTIM)*, pp. 16-25, May 24-26, 2012.

[4] L. Ängquist, A. Haider, H.-P. Nee, and H. Jiang, "Open-loop approach to control a Modular Multilevel Frequency Converter," in *Proc. 14th Eur. Conf. Power Electron. Appl. (EPE)*, pp. 1-10, Aug. 30-Sept. 1, 2011.

[5] L. Bessegato, L. Harnefors, K. Ilves, S. Norrga, and S. Östlund, "Control of direct AC/AC modular multilevel converters using capacitor voltage estimation," in *Proc. 18th Eur. Conf. Power Electron. Appl. (EPE)*, pp. 1-10, Sept. 5-9, 2016.

[6] M. Vasiladiotis, N. Cherix, and A. Rufer, "Operation and control of single-to-three-phase direct AC/AC Modular Multilevel Converters under asymmetric grid conditions," in *Proc. 9th Int. Conf. Power Electron. (ICPE)*, pp. 1-6, June 1-5, 2015.

[7] M. Vasiladiotis, N. Cherix, and A. Rufer, "Single-to-three-phase direct AC/AC Modular Multilevel Converters with Integrated Split Battery Energy Storage for Railway Interties," in *Proc. 17th Eur. Conf. Power Electron. Appl. (EPE)*, pp. 1-7, Sept. 8-10, 2015.

[8] K. Ilves, S. Norrga, and H.-P. Nee, "On energy variations in modular multilevel converters with full-bridge submodules for AC-DC and AC-AC applications," in *Proc. 15th Eur. Conf. Power Electron. Appl. (EPE)*, pp. 1-10, Sept. 2-6, 2013.

[9] D. Weiss, M. Vasiladiotis, C. Bănceanu, N. Drack, B. Ødegård, and A. Grondona, "IGCT-based modular multilevel converter for an AC-AC railway power supply," in *Proc. Conf. Power Electron. Intel. Motion (PCIM)*, pp. 1-8, May 16-18, 2017.

[10] N. Thitichaiworakorn, M. Hagiwara, and H. Akagi, "A single-phase to three-phase direct modular multilevel cascade converter based on double-star bridge-cells (MMCC-DSBC)," in *Proc. 1st Int. Future Energy Electron. Conf.*, pp. 476-481, Nov. 3-6, 2013.
[11] H.T. Mouton and B. Putzeys, "Understanding the PWM Nonlinearity: Single-Sided Modulation," *IEEE Trans. Power Electron.*, vol. 27, no. 4, pp. 2116-2128, Apr. 2012.
[12] T. Geyer, N. Oikonomou, G. Papafotiou, and F.D. Kieferndorf, "Model Predictive Pulse Pattern Control," *IEEE Trans. Ind. Appl.*, vol. 48, no. 2, pp. 663-676, Mar./Apr. 2012.
[13] A. Hassanpoor, L. Ängquist, S. Norrga, K. Ilves, and H.-P. Nee, "Tolerance Band Modulation Methods for Modular Multilevel Converters," *IEEE Trans. Power Electron.*, vol. 30, no. 1, pp. 311-326, Jan. 2015.

 ISBN: 9789075815276 et CFP17850-ART